Drones Practicing Mechanics

Harshvardhan Uppaluru¹, Mohammad Ghufran¹, Aeris El Asslouj², and Hossein Rastgoftar^{1,2}

Abstract — Mechanics of materials is a traditional engineering course that exposes undergraduate students in a variety of engineering fields to the principles of strain and stress analysis. However, material deformation and strain have been evaluated theoretically, numerically, and empirically tested using expensive machinery and instruments. This paper describes a novel method for analyzing strain and deformation using quadrotors. We propose to treat quadrotors as a finite number of particles of a deformable body and apply the principles of continuum mechanics to illustrate the concept of axial and shear deformation in 2-D and 3-D motion spaces. The outcome from this work has the potential to significantly impact undergraduate education by bridging the gap between classroom instruction and hardware implementation and experiments using quadrotors. Therefore, we introduce a new role for quadrotors as "teachers," which provides an excellent opportunity to practice theoretical concepts of mechanics in a productive way.

I. INTRODUCTION

Cooperative control and formation keeping are important areas of research into multi-agent systems (MAS) with several applications such as surveillance [1], search and rescue missions [2], precision agriculture [3], air traffic monitoring [4], area surveys [5] and payload delivery [6]. A MAS consisting of unmanned aerial vehicles can offer significant advantages over a single unmanned aerial vehicle (UAV) in terms of efficiency, costs, and resilience to failures. Cooperation amongst the agents in a MAS also enhances the team's ability to recover from anomalies.

A. Related Work

Virtual structure [7], [8], consensus [9], [10], [11], containment control [12], [13], [14] and continuum deformation [15] are some of the most studied methodologies for MAS control. Virtual structure [16], [17], [18] is a centralized multi-agent coordination approach at which the multi-agent formation is represented as a single structure translating as a rigid-body in a 3-D motion space. Consensus control is a decentralized approach with several coordination applications proposed such as leaderless multi-agent consensus [19], [20] and leader-follower consensus [21]. Fixed communication topology and switching inter-agent communication are other areas under multi-agent consensus control previously investigated [22], [23]. Stability of the consensus control in

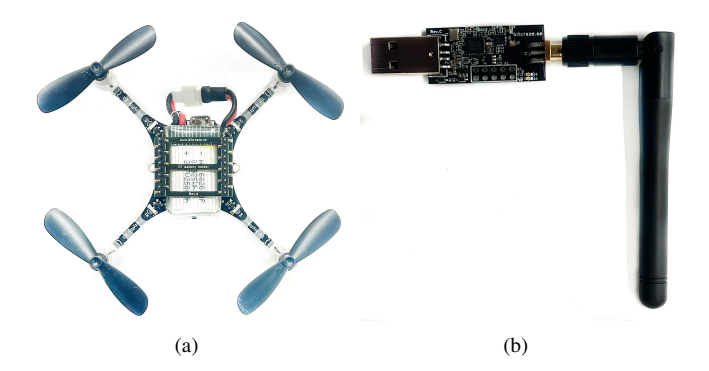


Fig. 1: (a) Crazyflie 2.1 (b) Loco Positioning Deck (c) Loco Positioning Node (d) Crazyradio PA

the presence of communication delays was also studied [24], [25].

Containment control is another decentralized leader-follower method where a finite number of leaders guide the followers through local communication. A finite-time containment control of a MAS was studied [26], [27]. Necessary and sufficient conditions for containment control stability and convergence were established in [28], [29]. Researchers have explored containment control under fixed and switching inter-agent communication [30]. Containment control under the presence of time-varying delays affecting multi-agent coordination was analyzed [31], [32].

Continuum deformation is another decentralized multiagent coordination approach that treats agents as particles of a continuum authorizing safe translation, rotation, and shear deformation of a MAS in a 3-D space under a homogeneous transformation. A n-D (n = 1, 2, 3) homogeneous transformation is defined by n+1 leaders in \mathbb{R}^n , located at the vertices of an n-D simplex at any time t, i.e. an n-D simplex is an n-D convex hull defined by n+1 leader agents. While leaders plan desired trajectories and move independently, the remaining follower agents obtain the desired trajectories, defined by the homogeneous transformation, through local communication. Though, continuum deformation and containment control are similar and both are decentralized leader-follower methods, continuum deformation ensures inter-agent collision avoidance, obstacle collision avoidance and agent containment by formally specifying and verifying safety in a large-scale agent coordination system [33], [34]. As a result, a large scale MAS can safely and aggressively deform using continuum deformation coordination. Experimental evaluation of continuum deformation coordination in 2-D with a team of 5 quadrotors was also performed [35].

^{*}This work has been supported by the National Science Foundation under Award Nos. 2133690 and 1914581.

¹Scalable Move and Resilient Traversability (SMART) Lab, University of Arizona, Tucson, Arizona, USA huppaluru, ghufran1942, hrastgoftar@arizona.edu

²Electrical and Computer Engineering Department, University of Arizona, Tucson, Arizona, USA aymaneelasslouj@arizona.edu

B. Contributions and Outline

This paper presents an approach for visualizing linear deformation in 2-D and 3-D motion spaces using quadrotors, treated as particles of a deformable body. By flight experiments, we visualize linear deformation, while assuring inter-agent collision avoidance by imposing lower bounds on the axial strains of the proposed continuum deformation coordination. While numerical and analytical methodologies are available for studying material deformation, our work presents a novel approach for analyzing material deformation and strain using quadrotors. This will provide a great opportunity for integration of robots into education by developing innovative techniques for teaching the fundamental ideas of mechanics in a practical manner. Additionally, by imposing the lower bound on the principle strains of the quadrotor team deformation, we can provide inter-quadrotor collision avoidance utilizing the proposed linear deformation coordination and strain analysis.

This paper is organized as follows: basics of linear deformation are presented in Section II. Our approach for software and hardware realization of the continuum deformation is detailed in Section III. The experimental setup, and flight test results are presented in Section IV and followed by Conclusion in Section V.

II. PRELIMINARIES

The linear transformation of a deformable body in a 3-D motion space, specified by a homogeneous transformation is given by,

$$\mathbf{r}_i(t) = \mathbf{Q}(t)\mathbf{r}_{i0} + \mathbf{d}(t), \qquad t \ge t_0, \tag{1}$$

where t_0 is the initial time, t is the current time, $\mathbf{r}_{i0} \in \mathbb{R}^3$ is the material position of particle i at time t_0 , $\mathbf{d}(t)$ is the rigid-body displacement vector, $\mathbf{r}_i(t)$ is the current desired position of particle i at time t. $\mathbf{Q}(t)$ is a Jacobian matrix that can be decomposed as follows:

$$\mathbf{Q}(t) = \mathbf{R}(t)\mathbf{E}(t), \qquad (2)$$

where $\mathbf{R}(t)$ is an orthogonal rotation matrix and $\mathbf{E}(t)$ is a positive definite strain matrix defined as

$$\mathbf{E}(t) = \begin{bmatrix} \epsilon_{xx}(t) & \epsilon_{xy}(t) & \epsilon_{xz}(t) \\ \epsilon_{xy}(t) & \epsilon_{yy}(t) & \epsilon_{yz}(t) \\ \epsilon_{xz}(t) & \epsilon_{yz}(t) & \epsilon_{zz}(t) \end{bmatrix}. \tag{3}$$

Before proceeding further, we make following assumptions:

Assumption 1. We assume that the material configuration of the continuum is the same as the initial configuration. Therefore, $\mathbf{r}_{i,0} = \mathbf{r}_i(t_0)$ i.e., material position \mathbf{r}_{i0} is the same as the initial position $\mathbf{r}_i(t_0)$ for every material particle i.

Assumption 2. We assume that the rigid-body displacement vector, $\mathbf{d}(t_0) = 0$.

Considering assumptions 1 and 2, \mathbf{Q} becomes the identity matrix at the initial time t_0 , i.e., $\mathbf{Q}(t_0) = \mathbf{I}_3$.

III. METHODOLOGY

We consider N quadrotors coordinating in a 3-D motion space where they are identified by set $\mathcal{V}=\{1,\cdots,N\}$. We define quadrotors as particles of a deformable body and let Eq. (1) define the desired continuum deformation of the quadrotor team. Without loss of generality, we only focus on realization of pure deformation, thus, we set $\mathbf{d}(t)=\mathbf{0}\in\mathbb{R}^{3\times 1}$ and $\mathbf{R}=\mathbf{I}\in\mathbb{R}^{3\times 3}$ at any time t i.e., rigid-body displacement and rotation are both zero at any time t. Under this assumption, the quadrotor team continuum deformation, given by (1), simplifies to

$$\mathbf{r}_{i}(t) = \mathbf{E}(t)\,\mathbf{r}_{i,0}, \qquad \forall i \in \mathcal{V}, \ \forall t \in [t_0, t_f]$$
 (4)

where t_0 and t_f denote the initial and final times. $\mathbf{r}_{i,0}$ and $\mathbf{r}_i(t)$ are the material and the current desired position of quadrotor $i \in \mathcal{V}$. Positive definite strain matrix $\mathbf{E}(t)$, defined by (3), specifies the axial strains and shear deformations in a linear deformation scenario.

While particles have infinitesimal size in a material deformation, here, quadrotors, treated as particles of a deformable body, are rigid and cannot deform. Therefore, realization of linear deformation by a quadrotor team requires to assure inter-agent collision avoidance via constraining the lower bound of the principal strains of matrix $\mathbf{E}(t)$ at any time t. To this end, the principal strains, defined as eigenvalues of matrix \mathbf{E} , must all be greater than ϵ_{min} where ϵ_{min} is obtained based on the following conditions:

- (i) quadrotor size,
- (ii) quadrotor trajectory control performance, and
- (iii) the minimum separation distance between every two quadrotors in the initial (material) configuration [15].

To assign ϵ_{min} , we will also make the following assumptions:

Assumption 3. Every quadrotor is enclosed by a ball of radius r

Assumption 4. The trajectory tracking error of every quadrotor is less than δ . Therefore,

$$\bigwedge_{i \in \mathcal{V}} (\|\mathbf{p}_i(t) - \mathbf{r}_i(t)\| \le \delta), \qquad \forall t \in [t_0, t_f], \qquad (5)$$

where $\mathbf{p}_i(t)$ is the actual position of quadrotor $i \in \mathcal{V}$ at time $t \in [t_0, t_f]$.

By imposing Assumptions 3 and 4, we obtain

$$\epsilon_{min} = \frac{2(\delta + r)}{p_{min}} \tag{6}$$

where p_{min} is the minimum separation distance between every two quadrotors in the initial configuration [15].

To formally characterize safety, we need to decompose matrix $\bf E$ and define it based on axial and shear strains. To this end, we use the 3-2-1 Euler angle standard to specify rigid-body rotation in a 3-D motion space by matrix

$$\mathbf{L}_{\mathrm{Euler}}\left(\phi,\theta,\psi\right) = \begin{bmatrix} c_{\theta}c_{\psi} & c_{\theta}s_{\psi} & -s_{\theta} \\ s_{\phi}s_{\theta}c_{\psi} - c_{\phi}s_{\psi} & s_{\phi}s_{\theta}s_{\psi} + c_{\phi}c_{\psi} & s_{\phi}c_{\theta} \\ c_{\phi}s_{\theta}c_{\psi} + s_{\phi}s_{\psi} & c_{\phi}s_{\theta}s_{\psi} - s_{\phi}c_{\psi} & c_{\phi}c_{\theta} \end{bmatrix}$$

where $c(.) = \cos(.)$, $s(.) = \sin(.)$, whereas ϕ , θ , and ψ are the first, second, and third Euler angles, respectively. Matrix $\mathbf{E}(t)$ can be decomposed as

$$\mathbf{E}(t) = \mathbf{L}_{\mathrm{Euler}}^{T}(\phi_{d}(t), \theta_{d}(t), \psi_{d}(t))$$

$$\times \mathbf{diag}(\epsilon_{1}(t), \epsilon_{2}(t), \epsilon_{3}(t))$$

$$\times \mathbf{L}_{\mathrm{Euler}}(\phi_{d}(t), \theta_{d}(t), \psi_{d}(t))$$
(7)

at any time $t \in [t_0, t_f]$, where $\phi_d(t)$, $\theta_d(t)$, $\psi_d(t)$ are the shear deformation angles and $\epsilon_1(t)$, $\epsilon_2(t)$, $\epsilon_3(t)$ are the strain values. The axial and shear strains specified by matrix $\mathbf{E}(t)$ can be graphically illustrated by using Mohr circle, as shown in Fig. 2. By using Mohr circle, we can assign the bounds on the deformation angles $\phi_d(t)$, $\theta_d(t)$, and $\psi_d(t)$ that will improve safety of the continuum deformation coordination.

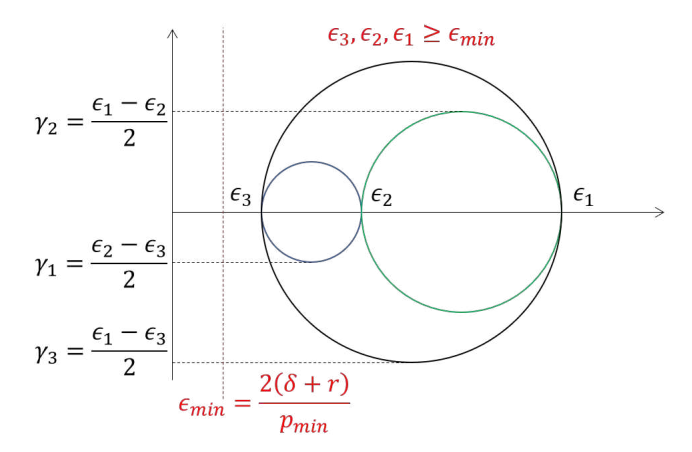


Fig. 2: Graphical representation of axial and shear strains by using Mohr circle.

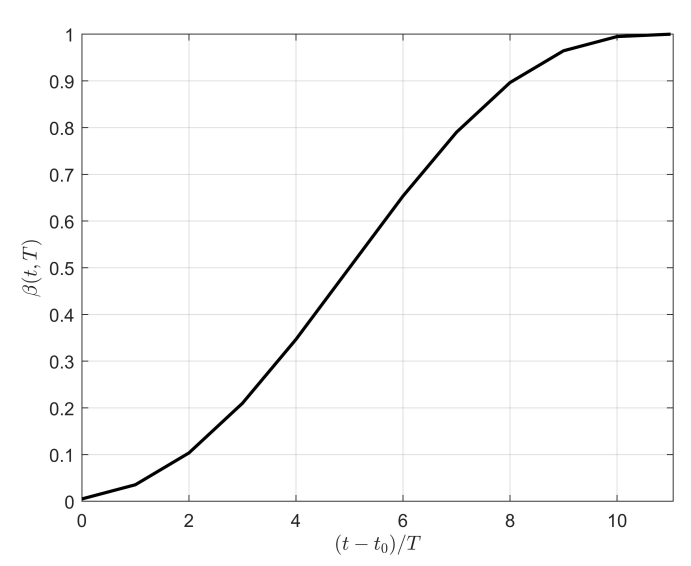


Fig. 3: $\beta(t,T)$ versus $\frac{t-t_0}{T}$ for $\frac{t-t_0}{T} \in [0,1]$.

For quadrotor team continuum deformation coordination, positive definite matrix $\mathbf{E}_f = \mathbf{E}\left(t_f\right) = \left[\epsilon_{ij}\left(t_f\right)\right]$ is known but final time t_f is free. The problem of continuum deformation planning consists of performing the following two steps:

• Step 1– Choosing Final Time t_f : The final time t_f needs to be sufficiently large such that the principal strains, denoted by ϵ_1 , ϵ_2 , and ϵ_3 , satisfy the following safety constraint:

$$\bigwedge_{i=1}^{3} \left(\epsilon_{min} \le \epsilon_i(t) \right), \qquad \forall t \in [t_0, t_f]. \tag{8}$$

In [36], it was shown that the minimum final time t_f^* can be obtained by using bi-section method such that all safety constraints are satisfied. To ensure condition (8) is satisfied, we choose a final time t_f that is greater than t_f^* .

- Step 2–Specifying $\mathbf{E}(t)$ for $t \in [t_0, t_f]$: To assure that the safety constraint (8) is satisfied at any time $t \in [t_0, t_f]$, we need to decompose matrix $\mathbf{E}(t)$ and perform the following steps to plan $\mathbf{E}(t)$ (for $t \in [t_0, t_f]$):
 - A. Assignment of Final Shear Deformation Angles and Ultimate Principal Strains: Given \mathbf{E}_f , we first obtain the final values of the shear deformation angles, denoted by $\phi_{d,f} = \phi_d(t_f)$, $\theta_{d,f} = \theta_d(t_f)$, and $\psi_{d,f} = \psi_d(t_f)$, and the ultimate principal strain values, denoted by $\epsilon_{1,f} = \epsilon_1(t_f)$, $\epsilon_{2,f} = \epsilon_2(t_f)$, and $\epsilon_{3,f} = \epsilon_3(t_f)$, by solving six non-linear equations provided by Eq. (7).
 - B. Planning of the Shear Deformation Angles and Principal Strains at Every Time $t \in [t_0, t_f]$: We first define the fifth order polynomial

$$\beta(t,T) = 6\left(\frac{t-t_0}{T}\right)^5 - 15\left(\frac{t-t_0}{T}\right)^4 + 10\left(\frac{t-t_0}{T}\right)^3$$
(9)

where $t\in[t_0,t_f],\,T=t_f-t_0$ is the travel time, $\beta\left(0,T\right)=0,\,\dot{\beta}\left(0,T\right)=\beta\left(t_f,T\right)=0,\,\ddot{\beta}\left(0,T\right)=\ddot{\beta}\left(t_f,T\right)=0,$ and $\beta\left(t_f,T\right)=1.$ The plot $\beta\left(t,T\right)$ versus $\frac{t-t_0}{T}$ is shown in Fig. 3. Then, the shear deformation angles and principal strains are defined by

$$\phi_d(t) = \phi_{d,0}(1 - \beta(t,T)) + \phi_{d,f}\beta(t,T),$$
 (10a)

$$\theta_d(t) = \theta_{d,0} (1 - \beta(t,T)) + \theta_{d,f} \beta(t,T),$$
 (10b)

$$\psi_d(t) = \psi_{d,0} (1 - \beta(t,T)) + \psi_{d,f} \beta(t,T),$$
 (10c)

$$\epsilon_1(t) = \epsilon_{1,0} (1 - \beta(t,T)) + \epsilon_{1,f} \beta(t,T), \quad (10d)$$

$$\epsilon_2(t) = \epsilon_{2,0} (1 - \beta(t,T)) + \epsilon_{2,f} \beta(t,T), \quad (10e)$$

$$\epsilon_3(t) = \epsilon_{3,0} (1 - \beta(t,T)) + \epsilon_{3,f} \beta(t,T), \quad (10f)$$

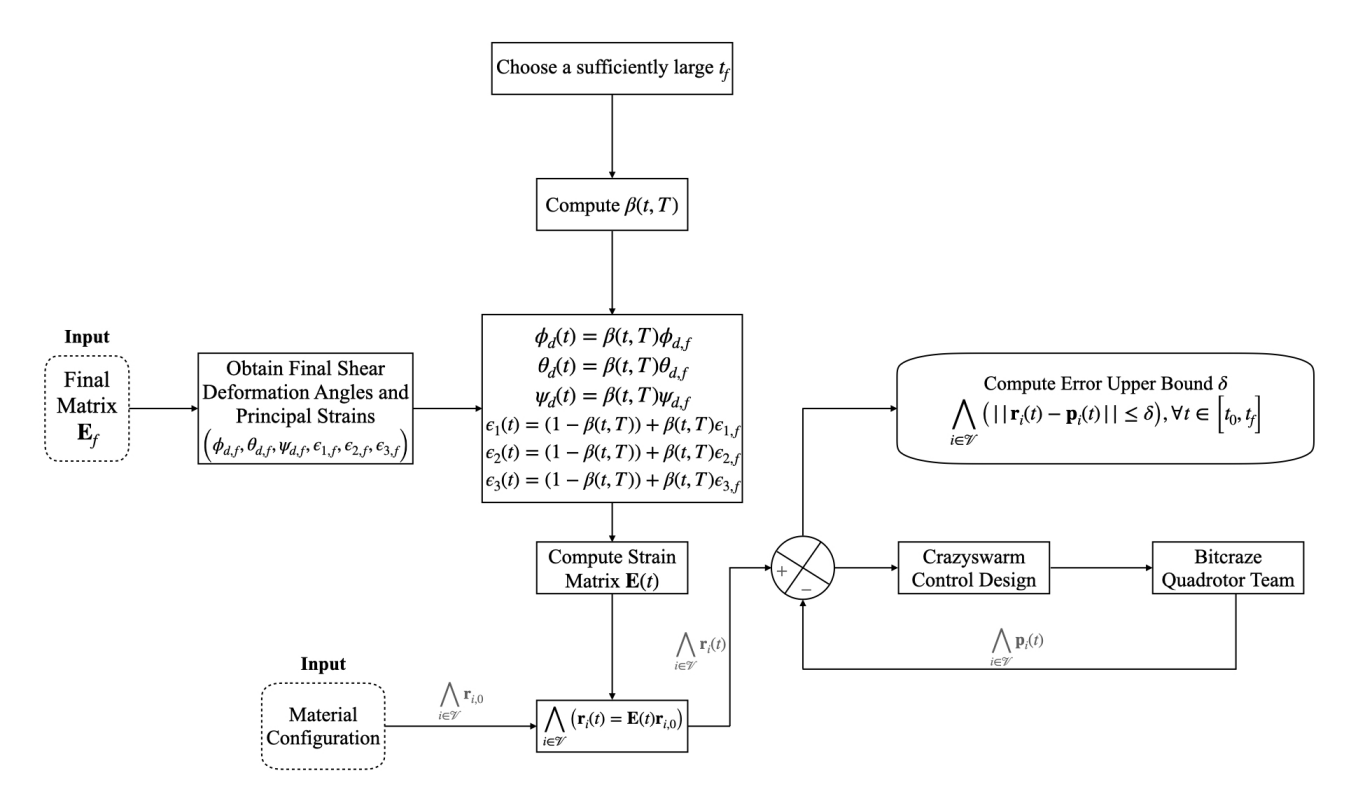


Fig. 4: The block diagram of quadrotor team coordination planning and control.

where $\phi_{d,0} = \phi_d(t_0) = 0$, $\theta_{d,0} = \theta_d(t_0) = 0$, $\psi_{d,0} = \psi_d(t_0) = 0$, $\epsilon_{1,0} = \epsilon_1(t_0) = 1$, $\epsilon_{2,0} = \epsilon_2(t_0) = 1$, and $\epsilon_{3,0} = \epsilon_3(t_0) = 1$ since $\mathbf{E}(t_0) = \mathbf{I} \in \mathbb{R}^{3\times 3}$ is an identity matrix (See Assumptions 1 and 2).

- C. Assignment of Matrix $\mathbf{E}(t)$: By knowing the shear deformation angles and principal strains at any time $t \in [t_0, t_f]$, matrix $\mathbf{E}(t)$ is assigned by using Eq. (7) at any time $t \in [t_0, t_f]$.

Functionality of our proposed approach for experimental evaluation of continuum deformation coordination is shown in Fig. 4.

Algorithm 1 2-D Safe Continuum Deformation Algorithm

```
Input r_0, \epsilon_{1,f}, \epsilon_{2,f}, \epsilon_{1,f}, \psi_{d,f}, t_f, and time increment h

Output r_d(t)

n_s \leftarrow \frac{t_f}{h}

Initialize \epsilon_{1,0} = 0, \epsilon_{2,0} = 0, \epsilon_{3,0} = 1, \psi_{d,0} = 1

for i = 1, 2, \cdots, n_s do

t \leftarrow i * h

Compute \beta using (9).

Get \epsilon_{1,i}, \epsilon_{2,i}, \epsilon_{3,i}, \psi_{d,i} using (10).

Compute \mathbf{E}(t) using (7).

\mathbf{r}_{i,d}(t) = \mathbf{E}(t)\mathbf{r}_0
end for
```

IV. EXPERIMENTS

In this section, the proposed approach was validated through both 2-D and 3-D flight tests. The hardware and soft-

```
Algorithm 2 3-D Safe Continuum Deformation Algorithm
```

```
Input r_0, \ \epsilon_{1,f}, \epsilon_{2,f}, \epsilon_{3,f}, \phi_{d,f}, \theta_{d,f}, \psi_{d,f}, \ t_f, and time increment h

Output r_d(t)

n_s \leftarrow \frac{t_f}{h}

Initialize \epsilon_{1,0} = 0, \epsilon_{2,0} = 0, \epsilon_{3,0} = 0, \phi_{d,0} = 1, \theta_{d,0} = 1, \psi_{d,0} = 1

for i = 1, 2, \cdots, n_s do

t \leftarrow i * h

Compute \beta using (9).

Get \epsilon_{1,i}, \epsilon_{2,i}, \epsilon_{3,i}, \phi_{d,i}, \theta_{d,i}, \psi_{d,i} using (10).

Compute \mathbf{E}(t) using (7).

\mathbf{r}_{i,d} = \mathbf{E}(i)\mathbf{r}_0
end for
```

ware configurations for the multi-quadrotor system (MQS) are summarized below, followed by a presentation of the test results. It should be noted that the Crazyflie (cf) quadrotor was utilized in our flight tests, so the terms "cf" and "quadrotor" are used interchangeably in this context.

1) Hardware and Software Configuration: The proposed continuum deformation coordination approach was evaluated on a hardware configuration consisting of Crazyflie 2.1¹ (See Fig. 1(a)), open-source, open-hardware nano quadrotor developed by Bitcraze². 4 coreless DC motors and 45 mm plastic propellers are included with each Crazyflie. As a

```
Inttps://www.bitcraze.io/products/crazyflie-2-1/
Inttps://www.bitcraze.io/
```

Parameter	2-D	3-D
$\epsilon_{1,f}$	1.8	0.9
$\epsilon_{2,f}$	0.8	1.1
$\epsilon_{2,f} \\ \epsilon_{3,f}$	1	0.7
$\phi_{d,f}$	0	0.1
$\theta_{d,f}$	0	0.12
$\psi_{d,f}^{-,j}$	-0.2	0.15

TABLE I: Shear deformation angles and principal strains.

result, the quadrotor is just $92\,\mathrm{mm}$ diagonal rotor-to-rotor, $29\,\mathrm{mm}$ tall, and weighs around $27\,\mathrm{g}$ with the battery, making it ideal for dense formation flight.

The Crazyflie (cf) quadrotor is equipped with two microcontroller units (MCUs): a Cortex-M4, 168MHz, 192kb SRAM, 1Mb flash primary controller, STM32F405, and a Cortex-M0, 32MHz, 16kb SRAM, 128kb flash controller, nRF5182. The primary application MCU is STM32F405, which is capable of inertial state estimation and control tasks, while nRF51822 is responsible for radio and power management. Each Crazyflie can fly for up to 7 minutes on a single charge of its 240mAh LiPo battery. Each cf connects with a PC through the Crazyradio PA³ (See Fig. 1(b)), a long range 2.4 GHz USB radio capable of sending up to 2 Mbps in 32-byte packets.

The Ground Control Station (GCS) is an Intel i7 11-th gen desktop, with 16 GB of RAM running Ubuntu 20.04. We employ ROS Noetic in conjunction with the Crazyswarm ROS stack built by the USC-ACT lab⁴ [37] for flight experiments. Crazyswarm platform enables the user to fly a swarm of crazyflie quadrotors with ease in tight formations. All flight tests were carried out at the University of Arizona's Scalable Move and Resilient Transversability (SMART) lab's indoor flying arena with a volume of $5\,\mathrm{m}\times5\,\mathrm{m}\times2\,\mathrm{m}$ equipped with 8 VICON motion capture cameras.

2) Discussion of the Initial Configuration: In Figs. 5 and 6, cf 1-2-3 form the outer triangle whereas cf 4-5-6 form the inner triangle. The distance between cfs 3-6 is the smallest, where $p_{min}=0.5\,\mathrm{m}$. At any time $t>t_0$ during the experiment, the inner triangle will always lie inside the outer triangle. Similarly, in case of 3-D as shown by Figs. 7 and 8, quadrotors 1-2-3-4 form the outer tetrahedron whereas quadrotors 5-6-7-8 form the inner tetrahedron. In this case, the distance between quadrotors 4-8 is the minimum where $p_{min}=0.3536\,\mathrm{m}$. Similar to the case in 2-D, the inner tetrahedron will always be inside the volume of the outer tetrahedron at all times $t>t_0$.

TABLE II: Initial positions of the quadrotor system.

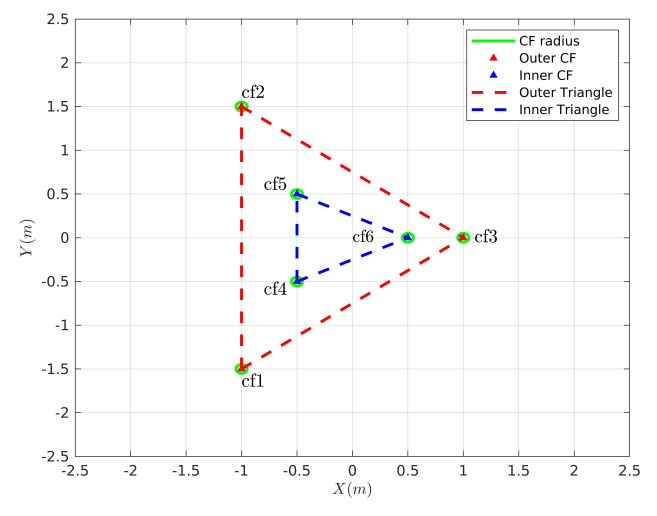


Fig. 5: Initial configuration of the quadrotor team consisting of 6 quadrotors in a 2-D continuum deformation coordination experiment. The exact coordinates (x-y) of each quadrotor has been provided in Table II. z-coordinate for all quadrotors is assumed to be constant and equal to $1 \, \mathrm{m}$ in this experiment.

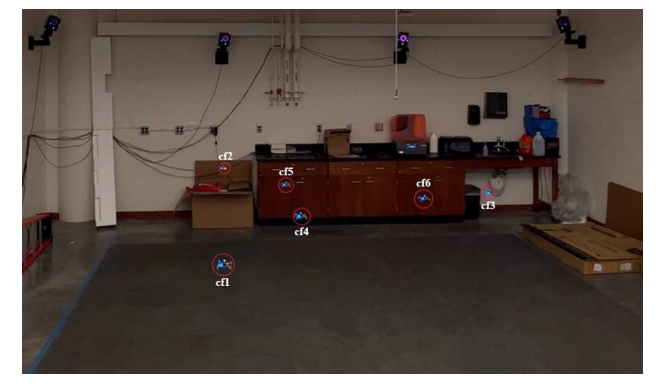


Fig. 6: Initial configuration for 2-D flight tests.

²⁻D (in m) 3-D (in m) $z_i(0)$ Quadro $x_i(0)$ $y_i(0)$ $x_i(0)$ $y_i(0)$ tor -1.00-1.50-1.75-1.500.75 2 -1.001.50 -1.751.50 0.753 1.00 0.0 2.00 0.00 0.75-0.50-0.500.00 1.75 4 -0.55 -0.500.5-0.75-0.501.00 6 0.500.00 -0.750.501.00 0.751.00 0.00-0.250.00 1.50

³https://www.bitcraze.io/products/crazyradio-pa/
4https://crazyswarm.readthedocs.io/en/latest/

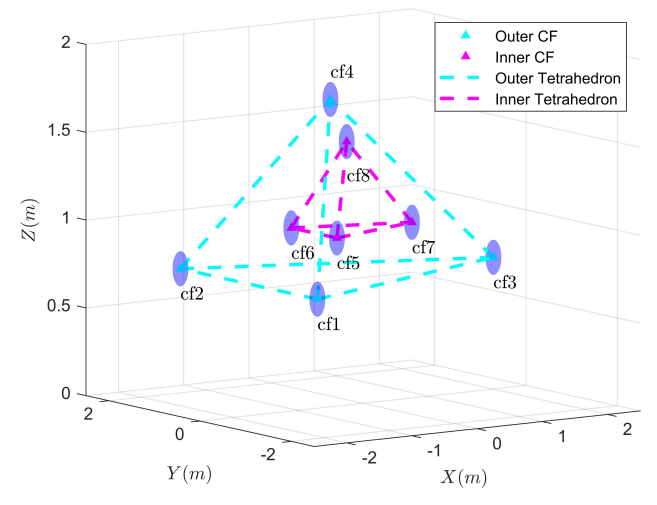


Fig. 7: Initial configuration of the quadrotor team consisting of 8 quadrotors in a 3-D continuum deformation coordination. The exact coordinates (x-y-z) of each quadrotor has been provided in Table II.

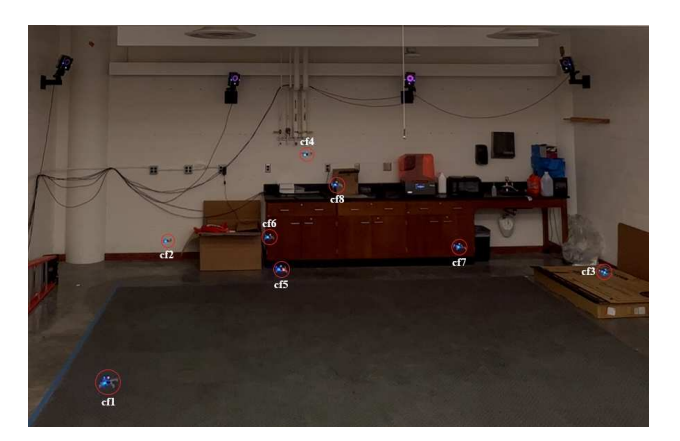


Fig. 8: Initial configuration for 3-D flight tests.

Figs. 9 and 10 show the desired trajectories for the 2-D and 3-D continuum deformation experiment for the multiquadrotor system (MQS) consisting 6 and 8 crazyflie respectively (See algorithm 1 for 2-D and algorithm 2 for 3-D). To ensure inter-quadrotor collision avoidance, the minimum separation distance in the initial configuration should be large enough such that the safety condition in Eq. (6) is satisfied. The tracking of quadrotors in an environment is accurate up to $0.05\,\mathrm{m}$. Therefore, we choose tracking error $\delta=0.05\,\mathrm{m}$, and obtain the following condition on the minimum separation distance in the initial configuration:

$$p_{min} \ge \frac{2 \times (\delta + r)}{\epsilon_{min}} = \frac{0.2}{\epsilon_{min}} \tag{11}$$

For the following flight experiments, we consider $t_f = 12s$.

3) 2-D Continuum Deformation Coordination Experiment: According to Table I, $\epsilon_{min}=0.8$ is considered for the 2-D continuum deformation experiment. Substituting the value of ϵ_{min} in Eq. (11), we get $p_{min}=0.25\,\mathrm{m}$. As listed in Table II, cf 3-6 are closest compared to any other pair

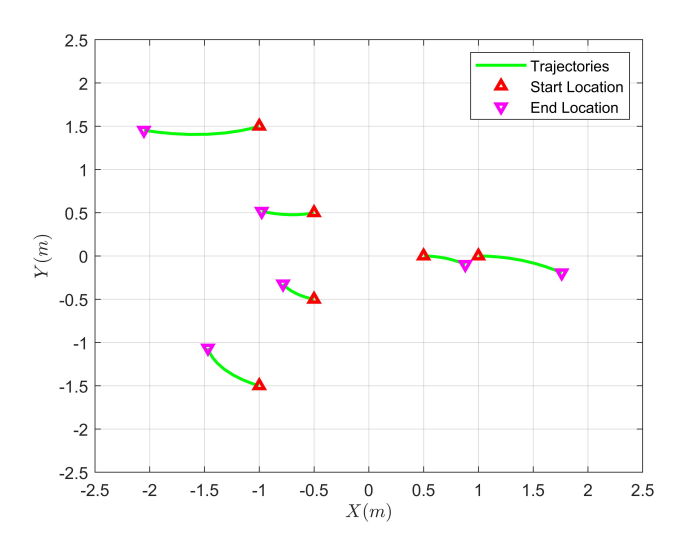


Fig. 9: Desired 2-D trajectories

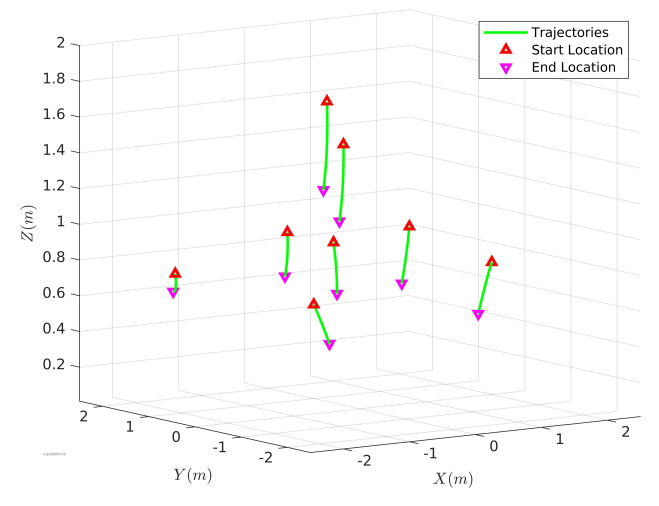


Fig. 10: Desired 3-D simulation results

of quadrotors. The distance between them is $0.5\,\mathrm{m}$ which satisfies Eq. (11), thus guaranteeing collision avoidance. Fig. 9 shows the desired trajectories whereas Fig. 11 shows the observed trajectories during our flight tests.

4) 3-D Continuum Deformation Coordination Experiment: According to Table I, we have $\epsilon_{min}=0.7$ for 3-D experiments. Substituting the value of ϵ_{min} in Eq. (11), we get $p_{min}=0.285\,\mathrm{m}$. We observe from Table II that cf pair 4-8 is closest. The distance between them is $0.3536\,\mathrm{m}$ which satisfies Eq. (11). Fig. 10 shows the desired trajectories whereas Fig. 12 shows the final trajectories obtained in our experiments.

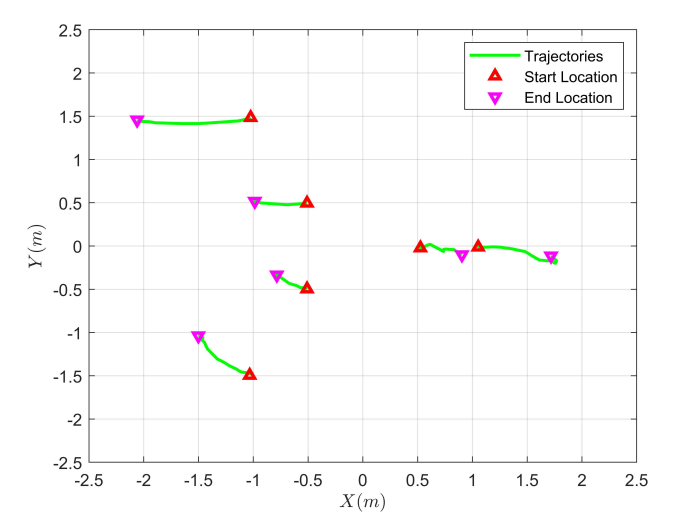


Fig. 11: Obtained trajectories of the quadrotor team in the 2-D continuum deformation coordination experiment.

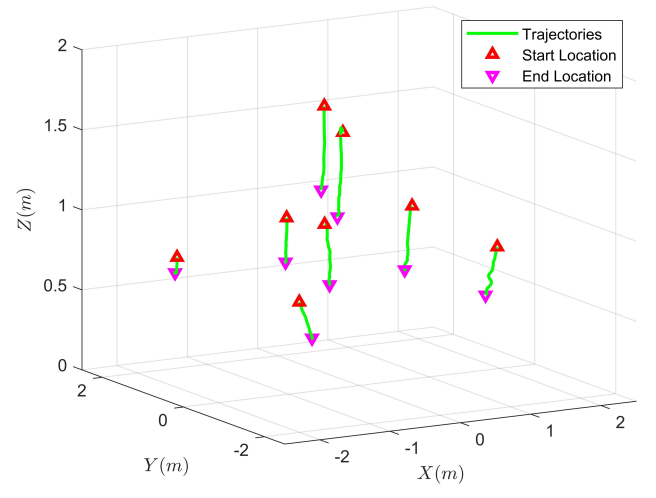


Fig. 12: Obtained trajectories of the quadrotor team in the 3-D continuum deformation coordination experiment.

V. CONCLUSION

In this paper, we treated quadrotors as particles of a deformable body and applied the principles of continuum mechanics to experimentally demonstrate the concept of linear deformation, principal strains, and shear strains. The primary objective of this work was to provide a new multidisciplinary learning approach for undergraduate students studying different engineering majors. By experimentally demonstrating linear deformation, principal strains, and shear strains, this work offered a novel visual perspective on mechanics education. The secondary objective of this work focused on experimentally validating via flight experiments, continuum deformation guidance protocol and show how a team of quadrotors can deform while assuring collision avoidance when they pass through narrow passages. The proposed methodology has the potential to open up new research opportunities and foster a deeper understanding of mechanics principles among engineering students.

REFERENCES

- M. K. Allouche and A. Boukhtouta, "Multi-agent coordination by temporal plan fusion: Application to combat search and rescue," *Information Fusion*, vol. 11, no. 3, pp. 220–232, 2010.
- [2] A. Kleiner, A. Farinelli, S. Ramchurn, B. Shi, F. Maffioletti, and R. Reffato, "Rmasbench: benchmarking dynamic multi-agent coordination in urban search and rescue," in 12th International Conference on Autonomous Agents and Multiagent Systems (AAMAS 2013). The International Foundation for Autonomous Agents and Multiagent Systems ..., 2013, pp. 1195–1196.
- [3] O. Ali, B. Saint Germain, J. Van Belle, P. Valckenaers, H. Van Brussel, and J. Van Noten, "Multi-agent coordination and control system for multi-vehicle agricultural operations." in AAMAS, 2010, pp. 1621– 1622.
- [4] H. Idris, K. Bilimoria, D. Wing, S. Harrison, and B. Baxley, "Air traffic management technology demonstration—3 (atd-3) multi-agent air/ground integrated coordination (maagic) concept of operations," NASA/TM-2018-219931, NASA, Washington DC, Tech. Rep., 2018.
- [5] J. Han, Y. Xu, L. Di, and Y. Chen, "Low-cost multi-uav technologies for contour mapping of nuclear radiation field," *Journal of Intelligent* & *Robotic Systems*, vol. 70, no. 1, pp. 401–410, 2013.
- [6] H. Rastgoftar and E. M. Atkins, "Cooperative aerial payload transport guided by an in situ human supervisor," *IEEE Transactions on Control Systems Technology*, vol. 27, no. 4, pp. 1452–1467, 2018.
- [7] W. Ren and R. Beard, "Virtual structure based spacecraft formation control with formation feedback," in AIAA Guidance, Navigation, and control conference and exhibit, 2002, p. 4963.
- [8] C. B. Low and Q. San Ng, "A flexible virtual structure formation keeping control for fixed-wing uavs," in 2011 9th IEEE international conference on control and automation (ICCA). IEEE, 2011, pp. 621– 626
- [9] W. Ren, R. W. Beard, and E. M. Atkins, "Information consensus in multivehicle cooperative control," *IEEE Control systems magazine*, vol. 27, no. 2, pp. 71–82, 2007.
- [10] W. Cao, J. Zhang, and W. Ren, "Leader-follower consensus of linear multi-agent systems with unknown external disturbances," *Systems & Control Letters*, vol. 82, pp. 64–70, 2015.
- [11] J. Shao, W. X. Zheng, T.-Z. Huang, and A. N. Bishop, "On leader-follower consensus with switching topologies: An analysis inspired by pigeon hierarchies," *IEEE Transactions on Automatic Control*, vol. 63, no. 10, pp. 3588–3593, 2018.
- [12] B. Li, Z.-q. Chen, Z.-x. Liu, C.-y. Zhang, and Q. Zhang, "Containment control of multi-agent systems with fixed time-delays in fixed directed networks," *Neurocomputing*, vol. 173, pp. 2069–2075, 2016.
- [13] Y.-P. Zhao, P. He, H. Saberi Nik, and J. Ren, "Robust adaptive synchronization of uncertain complex networks with multiple timevarying coupled delays," *Complexity*, vol. 20, no. 6, pp. 62–73, 2015.
- [14] G. Notarstefano, M. Egerstedt, and M. Haque, "Containment in leader-follower networks with switching communication topologies," *Automatica*, vol. 47, no. 5, pp. 1035–1040, 2011.
- [15] H. Rastgoftar, Continuum deformation of multi-agent systems. Springer, 2016.
- [16] M. A. Lewis and K.-H. Tan, "High precision formation control of mobile robots using virtual structures," *Autonomous robots*, vol. 4, no. 4, pp. 387–403, 1997.
- [17] B. J. Young, R. W. Beard, and J. M. Kelsey, "A control scheme for improving multi-vehicle formation maneuvers," in *Proceedings of the* 2001 American Control Conference.(Cat. No. 01CH37148), vol. 2. IEEE, 2001, pp. 704–709.
- [18] R. W. Beard, J. Lawton, and F. Y. Hadaegh, "A feedback architecture for formation control," in *Proceedings of the 2000 American Control Conference. ACC (IEEE Cat. No. 00CH36334)*, vol. 6. IEEE, 2000, pp. 4087–4091.
- [19] J. Qin, C. Yu, and B. D. Anderson, "On leaderless and leaderfollowing consensus for interacting clusters of second-order multiagent systems," *Automatica*, vol. 74, pp. 214–221, 2016.
- [20] C. Ding, X. Dong, C. Shi, Y. Chen, and Z. Liu, "Leaderless output consensus of multi-agent systems with distinct relative degrees under switching directed topologies," *IET Control Theory & Applications*, vol. 13, no. 3, pp. 313–320, 2019.
- [21] Y. Wu, Z. Wang, S. Ding, and H. Zhang, "Leader-follower consensus of multi-agent systems in directed networks with actuator faults," *Neurocomputing*, vol. 275, pp. 1177–1185, 2018.

- [22] H. Wang, W. Yu, G. Wen, and G. Chen, "Fixed-time consensus of nonlinear multi-agent systems with general directed topologies," *IEEE Transactions on Circuits and Systems II: Express Briefs*, vol. 66, no. 9, pp. 1587–1591, 2018.
- [23] G. Wen, J. Huang, C. Wang, Z. Chen, and Z. Peng, "Group consensus control for heterogeneous multi-agent systems with fixed and switching topologies," *International Journal of Control*, vol. 89, no. 2, pp. 259–269, 2016.
- [24] J. Zhou, C. Sang, X. Li, M. Fang, and Z. Wang, "H-infinity consensus for nonlinear stochastic multi-agent systems with time delay," *Applied Mathematics and Computation*, vol. 325, pp. 41–58, 2018.
- [25] X. Zhang, Y. Huang, L. Li, Y. Wang, and W. Duan, "Delay-dependent stability analysis of modular microgrid with distributed battery power and soc consensus tracking," *IEEE Access*, vol. 7, pp. 101125– 101138, 2019.
- [26] X. Wang, S. Li, and P. Shi, "Distributed finite-time containment control for double-integrator multiagent systems," *IEEE Transactions* on *Cybernetics*, vol. 44, no. 9, pp. 1518–1528, 2013.
- [27] H. Liu, L. Cheng, M. Tan, Z. Hou, and Y. Wang, "Distributed exponential finite-time coordination of multi-agent systems: containment control and consensus," *International Journal of Control*, vol. 88, no. 2, pp. 237–247, 2015.
- [28] Y. Cao, W. Ren, and M. Egerstedt, "Distributed containment control with multiple stationary or dynamic leaders in fixed and switching directed networks," *Automatica*, vol. 48, no. 8, pp. 1586–1597, 2012.
- [29] M. Ji, G. Ferrari-Trecate, M. Egerstedt, and A. Buffa, "Containment control in mobile networks," *IEEE Transactions on Automatic Control*, vol. 53, no. 8, pp. 1972–1975, 2008.
- [30] W. Li, L. Xie, and J.-F. Zhang, "Containment control of leader-following multi-agent systems with markovian switching network topologies and measurement noises," *Automatica*, vol. 51, pp. 263–267, 2015.
- [31] J. Shen and J. Lam, "Containment control of multi-agent systems with unbounded communication delays," *International Journal of Systems Science*, vol. 47, no. 9, pp. 2048–2057, 2016.
- [32] K. Liu, G. Xie, and L. Wang, "Containment control for second-order multi-agent systems with time-varying delays," *Systems & Control Letters*, vol. 67, pp. 24–31, 2014.
- [33] H. Rastgoftar, E. M. Atkins, and D. Panagou, "Safe multiquadcopter system continuum deformation over moving frames," *IEEE Transac*tions on Control of Network Systems, vol. 6, no. 2, pp. 737–749, 2018.
- [34] H. Rastgoftar and E. M. Atkins, "Safe multi-cluster uav continuum deformation coordination," *Aerospace Science and Technology*, vol. 91, pp. 640–655, 2019.
- [35] M. Romano, P. Kuevor, D. Lukacs, O. Marshall, M. Stevens, H. Rast-goftar, J. Cutler, and E. Atkins, "Experimental evaluation of continuum deformation with a five quadrotor team," in 2019 American Control Conference (ACC). IEEE, 2019, pp. 2023–2029.
- [36] H. Rastgoftar and I. V. Kolmanovsky, "Safe affine transformation-based guidance of a large-scale multi-quadcopter system (mqs)," *IEEE Transactions on Control of Network Systems*, 2021.
- [37] J. A. Preiss*, W. Hönig*, G. S. Sukhatme, and N. Ayanian, "Crazyswarm: A large nano-quadcopter swarm," in *IEEE International Conference on Robotics and Automation (ICRA)*. IEEE, 2017, pp. 3299–3304, software available at https://github.com/USC-ACTLab/crazyswarm. [Online]. Available: https://doi.org/10.1109/ICRA.2017.7989376